Relative Role of Turbulent and Radiative Flux on the Near-Surface Temperature in a Single-Layer Urban Canopy Model over Houston

JAMES BROWNLEE AND PALLAV RAY

Department of Ocean Engineering and Sciences, Florida Institute of Technology, Melbourne, Florida

MUKUL TEWARI

The Weather Company, IBM T. J. Watson Research Center, New York, New York

HAOCHEN TAN

Department of Ocean Engineering and Sciences, Florida Institute of Technology, Melbourne, Florida

(Manuscript received 3 April 2017, in final form 17 May 2017)

ABSTRACT

Numerical simulations without hydrological processes tend to overestimate the near-surface temperatures over urban areas. This is presumably due to underestimation of surface latent heat flux. To test this hypothesis, the existing single-layer urban canopy model (SLUCM) within the Weather Research and Forecasting Model is evaluated over Houston, Texas. Three simulations were conducted during 24–26 August 2000. The simulations include the use of the default ''BULK'' urban scheme, the SLUCM without hydrological processes, and the SLUCM with hydrological processes. The results show that the BULK scheme was least accurate, and it overestimated the near-surface temperatures and winds over the urban regions. In the presence of urban hydrological processes, the SLUCM underestimates these parameters. An analysis of the surface heat fluxes suggests that the error in the BULK scheme is due to a lack of moisture at the urban surface, whereas the error in the SLUCM with hydrological processes is due to increases in moisture at the urban surface. These results confirm earlier studies in which changes in near-surface temperature were primarily due to the changes in the turbulent (latent and sensible heat) fluxes in the presence of hydrological processes. The contribution from radiative flux was about one-third of that from turbulent flux. In the absence of hydrological processes, however, the results indicate that the changes in radiative flux contribute more to the near-surface temperature changes than the turbulent heat flux. The implications of these results are discussed.

1. Introduction

To study weather and climate patterns around cities, it is critical that numerical models capture, in great detail, the changes in the urban atmosphere. Many of these changes are affected by the urban heat island (UHI) effect (Kalnay and Cai 2003). Such effects include local enhancement of thunderstorms and lightning patterns over cities (Westcott 1995; Bornstein and Lin 2000; Craig and Bornstein 2002; Rozoff et al. 2003); increases in heat stress (Zhang et al. 2011); and changes in the temperature, humidity, and winds at local and regional scale (Chen et al. 2011b; Lee et al. 2011). Other significant effects include increases in the depth of the urban planetary boundary layer (PBL; Hjelmfelt 1982; Lee et al. 2011; Zhang et al. 2011), changes in the dispersion of air pollution (Chen et al. 2004), and increased tropospheric ozone over cities (Weaver et al. 2009).

One way to incorporate these changes in an atmospheric model is to integrate the model at very high spatial and temporal resolutions. However, this approach is computationally demanding. An alternative to this approach is to develop urban parameterizations for the model. In the last decade, great progress had been made at developing and using urban parameterizations to diagnose the effects of enhanced urban development on local and regional weather patterns. Traditionally, urban surfaces in land surface models have been implemented using an approach similar to the ''big leaf'' method for vegetated surfaces

Corresponding author: Dr. Pallav Ray, pray@fit.edu

DOI: 10.1175/JAMC-D-17-0088.1

(Deardorff 1978; Walko et al. 2000; Mestayer et al. 2005; Rotach et al. 2005). This type of approach assumes that the urban surface is homogeneous throughout the city without any variation in building density or type. Over the last decade, the development of urban canopy models (UCMs) has largely moved beyond this simplistic approach, and the models have been developed with detailed representations of buildings, vegetation, and roads at the urban surface (e.g., Kusaka et al. 2001; Martilli et al. 2002; Lee and Park 2008; Oleson et al. 2008).

Many of the new urban parameterization advancements and developments have been for numerous models (e.g., The Town Energy Balance Model; Bueno et al. 2012) apart from the Advanced Research version of Weather Research and Forecasting (WRF) Model (WRF-ARW; Skamarock et al. 2008). Within WRF 3.7, there are four urban parameterizations: the bulk urban parameterization (''BULK''; Tewari et al. 2004; Liu et al. 2006), the single-layer urban canopy model (SLUCM; Kusaka et al. 2001), the multilayer urban canopy or building energy prediction model (BEP; Martilli et al. 2002), and the BEP plus indoor–outdoor exchange building energy model (BEM; Salamanca et al. 2011).

Both the BULK and SLUCM parameterizations are simulated in conjunction with the Noah land surface model (LSM; Chen and Dudhia 2001) in WRF. The primary function of the Noah LSM is to provide surface fluxes and skin temperatures at the lower boundary for coupled land–atmosphere models over natural and artificial/urban surfaces (Chen et al. 2011a). When the BULK scheme is used, it assumes that the entire urban region is impervious (Yang et al. 2014); thus, the physical parameterization is the same for both the urban and natural surfaces. The BULK scheme characterizes typical biophysical properties of urban areas such as albedo and emissivity. On the other hand, in urban canopy models, a representative urban canopy is considered.

The default Noah LSM within WRF has a very low green vegetation fraction and leaf area index (LAI) in urban areas (Lee et al. 2011). When these settings are used, the BULK scheme underestimates surface latent heat flux Q_{LH} and overestimates the surface sensible heat flux Q_{SH}. This is due to a lack of evaporation from the surface, which leads to lower Q_{LH} and higher surface temperature T_S. This higher T_S typically leads to higher Q_{SH} and a deeper PBL.

Lee et al. (2011) confirmed this when they used the default Noah LSM, a modified Noah LSM in which the surface vegetation was increased in the city, and the SLUCM over Houston, Texas. When the default Noah LSM was used, the simulated surface temperatures were about 1°–2°C higher than observed temperatures. Also, the simulated Q_{SH} (Q_{LH}) was higher (lower) than observations. The lower Q_{LH} indicates that not enough surface evaporation was occurring in their model. In addition to that, the PBL height was about 200–400 m higher than observations. When the surface vegetation was increased in the Noah LSM, the Q_{SH} was reduced, the Q_{LH} increased, and the PBL height decreased and became closer to the observations (Lee et al. 2011).

In the SLUCM, the urban surface is treated as a combination of natural and impervious surfaces (Yang et al. 2014), and it is coupled to the Noah LSM through a parameter known as the urban fraction (Chen et al. 2011a). The SLUCM calculates the fluxes over the paved or developed urban surfaces, and the Noah LSM calculates the fluxes over the natural surfaces like trees and parks. Thus, the total estimated surface flux is a combination of the impervious and natural surfaces coming from the estimates of the SLUCM and Noah LSM models (Chen et al. 2004, 2011a; Yang et al. 2015).

Despite these successes with the SLUCMs, they have considerable difficulty in simulating Q_{LH} (e.g., Grimmond et al. 2010, 2011) because the SLUCM oversimplifies complex urban hydrological processes within a city (Yang et al. 2015). Recently, great efforts have been made to improve the SLUCM by incorporating the following five new urban hydrological processes (Wang et al. 2011, 2013; Yang et al. 2015): anthropogenic latent heat flux, urban oasis effect, urban irrigation, evaporation from paved surfaces, and multilayer green roofs (see section 2 for details).

The first objective of this study is to evaluate the role of these new hydrological processes on the near-surface temperature and winds over Houston. Our second but primary objective is to address a question that is often overlooked in the literature: Is it the turbulent or radiative fluxes that contribute more to the near-surface temperature changes? Section 2 describes the model, the new hydrological processes in the WRF, methods, and data, followed by comparisons of model and observed 2-m temperature, 10-m winds, and surface heat fluxes in section 3. The discussion and conclusions are presented in section 4.

2. Model, data, and methods

a. Hydrological processes

The updated SLUCM in WRF 3.7 incorporates five new urban hydrological processes that are briefly discussed here.

1) ANTHROPOGENIC LATENT HEAT FLUX

The anthropogenic latent heat flux option adds the latent heat flux release from cooling systems as part of the total Q_{LH} in this updated SLUCM (Yang et al. 2015).

Moriwaki et al. (2008) have shown that a significant portion of the Q_{LH} in cities comes from water vapor emissions from cooling systems.

2) URBAN OASIS EFFECT

The enhancement in evapotranspiration rates within vegetated areas in a city is known as the "urban oasis effect." Within city environments, there are isolated patches of vegetation like trees and hedges, and unlike vegetation patches within forests, there is often full exposure to incoming radiation and wind. This leads to an enhancement of the evapotranspiration rate (Yang et al. 2015). For example, Oke (1979) found that evapotranspiration rates from an urban lawn were about 1.3 times greater than a rural patch of land.

3) URBAN IRRIGATION

Urban irrigation refers to the watering of various plants in a city through watering systems like automatic sprinklers. Urban irrigation was first implemented in the WRF Model by Georgescu et al. (2011). In the updated SLUCM, the urban irrigation is set to occur during a 2-h period from 1800 to 2000 local standard time (LST) each day from May to September (Yang et al. 2015). During these daily 2-h periods, moisture is added to the top two layers of the soil. When irrigated, volumetric moisture of the top two soil layers (0.4 m thick) of urban lawns or green roofs is set to reach a threshold value of 0.33 where transpiration is not limited by water availability. Such treatment is used to broadly represent, rather than exactly match, urban irrigation schemes in a variety of cities.

4) EVAPORATION FROM PAVED SURFACES

The evaporation from water-holding paved surfaces can contribute to a significant portion of the total moisture flux in an urban environment (Ramamurthy and Bou-Zeid 2014). The original SLUCM in WRF neglects storage and evaporation from paved surfaces after heavy rainfall events. The updated SLUCM allows evaporation processes from engineered surfaces both during and after rainfall events (Yang et al. 2015).

5) MULTILAYER GREEN ROOFS

The improved SLUCM incorporates three new layers on the roof: a vegetation soil layer, a growing medium layer, and a drainage layer (Yang et al. 2015). All three of these layers are included on top of a concrete roof deck. With the inclusion of the above hydrological processes, the updated SLUCM is expected to better capture the observed variation of near-surface temperature and surface fluxes (Yang et al. 2015; Miao and Chen 2014; Yang et al. 2016; Sharma et al. 2016). We have not used this option for this paper.

b. Model and simulation design

The WRF 3.7 was configured with three domains over Houston (Fig. 1). The innermost domain (1-km grid spacing) covers the urban areas in Houston including the observational points (see section 2c) for model validation. There were 35 sigma levels with the model top at 50 hPa. The lowest layer was ~35 m thick, and there were eight layers in the lowest 1 km. The time step was 30 s for the parent domain. Model initial and boundary conditions, including the sea surface temperature (SST), were provided by the National Centers for Environmental Prediction (NCEP) final analysis (NCEP_fnl, 1° × 1°, 6-hourly). The urban land-use data were obtained from the 30-m resolution 2001 National Land Cover Database (NLCD). Four simulations were conducted; they were initiated at 0000 UTC 24 August 2000 and integrated until 1800 UTC 26 August 2000. The frequency of the output was every 10 min. We have used default values of parameters that are provided in the model.

To study the effects of urban hydrological processes, three different urban configurations were used (Table 1). These different urban configurations were integrated with both the BULK (Tewari et al. 2004) and the original SLUCM (Kusaka et al. 2001) urban schemes. The other important parameterizations used in this study are (i) the Noah LSM (Chen and Dudhia 2001), (ii) the Mellor–Yamada–Janjić (MYJ) PBL scheme (Janjić 1994), (iii) the WSM3 (Hong et al. 2004) microphysics scheme, and (iv) the longwave Rapid Radiative Transfer Model (RRTM; Mlawer et al. 1997) and Dudhia (1989) shortwave radiation. Since the inner domains were simulated at horizontal resolutions of 3 and 1 km, no cumulus parameterization was used. Whereas, for the parent domain, the Kain–Fritsch cumulus parameterization (Kain 2004) was used. All of the model configurations and physical parameterizations that were used for this study are summarized in Table 2.

c. Data and method

The model simulations were validated with observations recorded at Texas Commission on Environmental Quality (TCEQ) air quality monitoring stations in Houston. The primary meteorological data that these stations record are near-surface temperature, wind speed, relative humidity, and dewpoint. Many of the stations had missing or inconsistent relative humidity and dewpoint data, so the primary focus of our analysis involved comparing the WRF 2-m temperature and 10-m wind speeds with the TCEQ observations. The TCEQ provides hourly averaged data. So for comparison purposes, the model output was also hourly averaged.

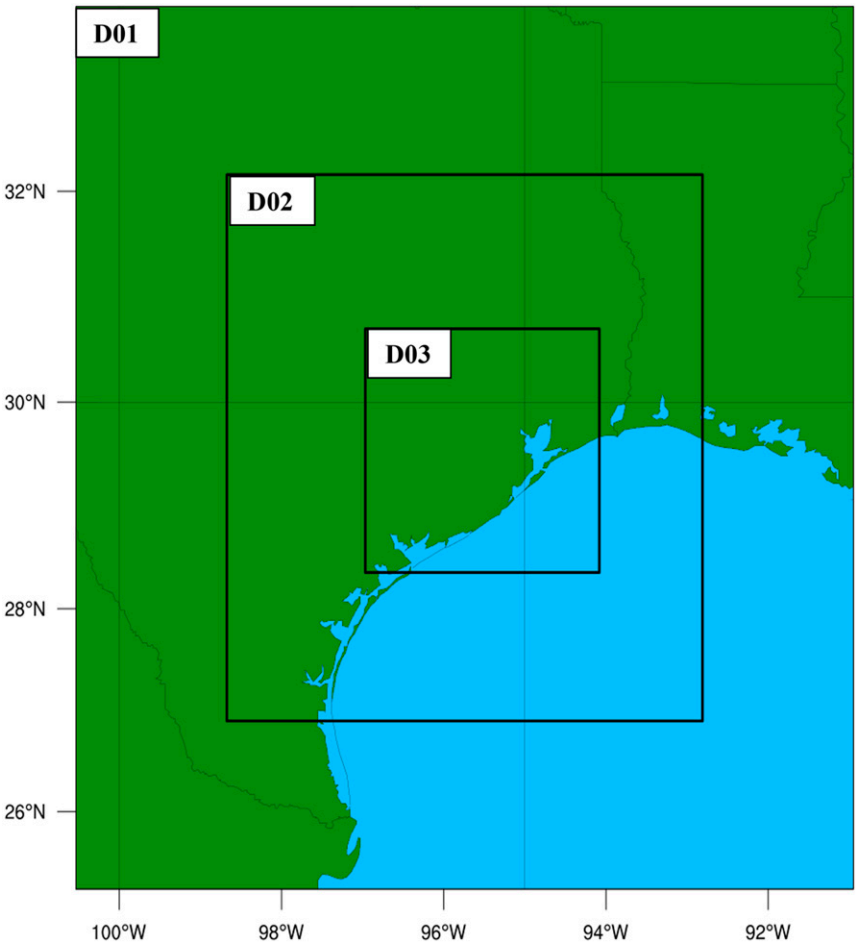

FIG. 1. WRF domain configuration. The outer domain has a 104 × 106 mesh with a horizontal resolution of 9 km, the second domain has a 190 × 196 mesh at 3 km, and the innermost domain has a 280 × 262 mesh at 1 km.

The TCEQ stations were segregated and grouped based on the dominant land-use categories as defined by the 2001 NLCD data (Fig. 2). The differences between the 2001 NLCD and 2006 NLCD data over Houston is minimal (not shown). The four general land categories, used here, are natural or rural (RUR) surfaces, low-intensity residential (LIR), high-intensity residential (HIR), and commercial/industrial (COI). In total, there are 18 surface stations (Fig. 2); 12 of them are in the urban land-use category, and 6 stations are in the rural land-use category. Of the 12 stations in the urban land category, 5 are located in both the LIR and COI categories, and 2 stations are located in the HIR category. The observations and model output were averaged across all stations in each land-use category. The model validation is performed for the 24-h period from

TABLE 1. Summary of urban configurations used in model simulations.

Expt	Hydrological options	Purpose
BULK	Has no urban hydrological options	Used as a benchmark for comparison with the new SLUCM with urban hydrological processes
SLUCM1	No hydrological options were used	Used as a benchmark for comparison with the new urban hydrological processes
SLUCM2	Hydrological options used are the anthropogenic Q_{LH}, urban oasis effect, urban irrigation, and evaporation from paved surfaces	To study the relationship between surface moisture increases and changes in the near-surface temperatures and wind speeds

TABLE 2. Model configuration and physical parameterizations used in the model simulations.

Category	Model setup
Horizontal resolution	D1: $dx = dy = 9$ km (104 × 106) D2: $dx = dy = 3$ km (190 × 196) D3: $dx = dy = 1$ km (280 × 262)
Vertical levels	35
Model top	50 hPa
Time step	30 s
PBL	MYJ (Janjić 1994)
Land surface	Noah LSM (Chen and Dudhia 2001)
Urban physics	Bulk (Tewari et al. 2004) Single-layer UCM (Kusaka et al. 2001)
Shortwave radiation	Dudhia (1989)
Longwave radiation	RRTM (Mlawer et al. 1997)
Cloud microphysics	WSM3 (Hong et al. 2004)
Cumulus parameterization	Kain–Fritsch (Kain 2004) in D1
Initial and boundary conditions	NCEP final analysis
Land use	NLCD
Simulation period	From 0000 UTC 24 to 1800 UTC 26 Aug 2000

1200 UTC [0700 central daylight time (CDT)] 25 to 1200 UTC (0700 CDT) 26 August 2000. The model simulations are evaluated during this time period because 25 August was a day characterized by a stable air mass with little organized convection (Nielsen-Gammon 2002; Cheng and Byun 2008). This helps to avoid complexities associated with moist convection since our primary goal here is to evaluate the role of the new urban canopy model.

3. Results

a. Evaluation of near-surface temperatures and winds

To fully appreciate the role of new hydrological processes on the urban environment, the BULK scheme results are discussed first. Figure 3 shows the averaged 2-m temperature (Figs. 3a–d) and 10-m winds (Figs. 3e–h) based on all stations in each of the four land categories. In the BULK, the temperature within the urban (Fig. 3a), COI–HIR (Fig. 3c), and LIR (Fig. 3d) land categories are considerably higher than the observations. Over the urban land category, the mean temperature is 1.43°C (Table 3) higher than the observations and for the COI–HIR and LIR categories, the mean temperature is 1.12°C (COI–HIR) and 1.87°C (LIR) higher than the observations, respectively. These positive mean biases in the temperature cause the highest RMSEs among the four urban configurations in all three urban land categories (Table 3) and is consistent with previous studies (e.g., Lee et al. 2011; Yang et al. 2014).

Within the rural land category, the BULK 2-m temperatures are slightly below the observations, as reflected in the negative mean biases, and the RMSE value is much smaller than the urban stations (Table 3). A similar trend occurs with the wind speeds (Figs. 3e–h). The BULK winds in the urban land category are 1.05 m s^{-1} higher than the observed winds, and the COI–HIR and LIR winds fall just below and above this number, respectively (Table 4). In the BULK, not only are the peak afternoon winds higher than the urban land category observations, they remain elevated into the night, 0600 to 1200 UTC (0100 to 0700 LST) 26 August (Figs. 3e,g,h). This is consistent with Lee et al. (2011) and Chen et al. (2011b), where they showed elevated near-surface wind speeds extending into the night. The winds from the BULK are smaller in the rural land category and are close to the observations (Table 4).

In the sensitivity experiment SLUCM1, there is a decrease in simulated temperature relative to the BULK for the urban land category (Figs. 3a,c,d). The positive mean bias in the BULK temperature within the urban land areas becomes slightly negative in the SLUCM1, and the RMSE decreases (Table 3). This reduction in temperature is especially dramatic in the LIR land category (Table 3). Clearly, the SLUCM1 greatly reduces the temperature, which becomes lower than the observed temperature with a negative bias of −0.34°C (Table 3). In contrast, an earlier study by Chen et al. (2011b) found temperatures that were nearly 1°C higher than the observations within the city. This discrepancy is possibly due to the use of different physics options. However, in our study, the possibility of a systematic error in the observed temperature cannot be ruled out.

In the rural land category, the RMSE increases as the SLUCM1 temperatures fall even further below the observations (Table 3). Within the rural land category, the winds in the BULK and SLUCM1 are similar (Table 3) since the rural areas are represented identically in our simulations. In contrast, within both the urban land categories, there is a noticeable decrease in the near-surface winds (Figs. 3e,g,h), which is reflected in the change in the mean biases in the three urban land categories (Table 4).

When the urban hydrological processes are included in the SLUCM2, the near-surface temperature falls slightly within all three urban land areas (Figs. 3a,c,d). The negative mean bias in the temperature in the city increases slightly with both configurations (Table 3). As a result, the temperature RMSE increases as the model temperatures fall further below the observations.

For winds, in the presence of urban hydrological processes, there is only a slight reduction from the SLUCM1 (Table 4). Clearly, this change in wind speeds

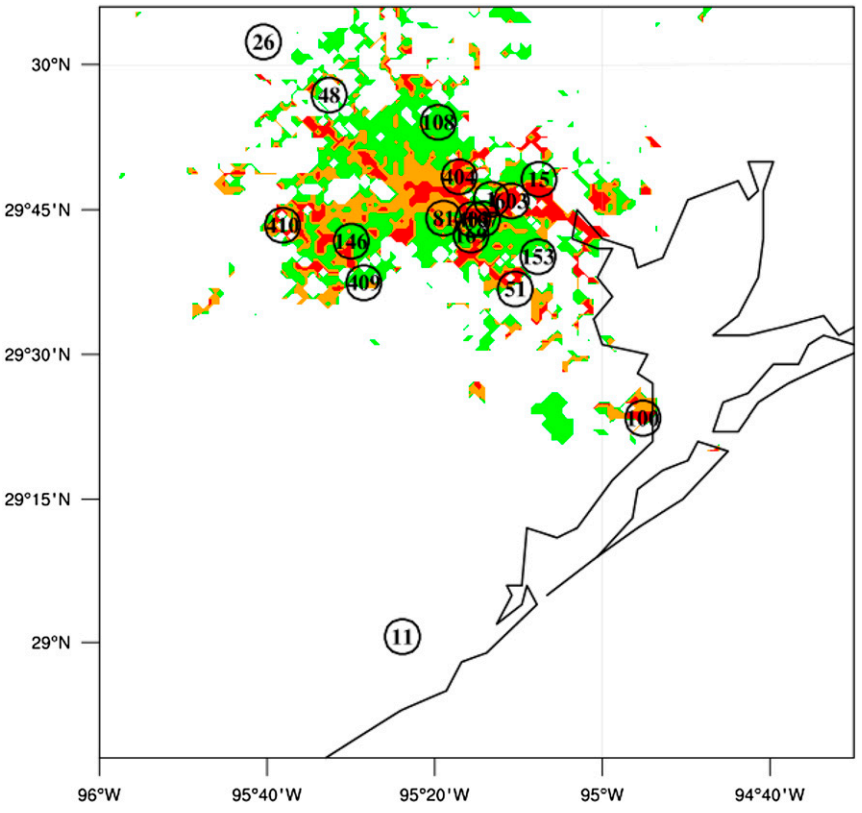

FIG. 2. Urban land-use categories (shaded) indicating LIR (green), HIR (orange), COI (red), and RUR (white). The ocean is also labeled as white. TCEQ station locations are circled. Urban TCEQ stations are 1, 15, 81, 100, 108, 146, 167, 169, 403, 404, 409, and 603; rural stations are 11, 26, 48, 51, 153, and 410; COI–HIR stations are 81, 100, 146, 167, 403, 404, and 603; and LIR stations are 1, 15, 108, 169, and 409.

is much less dramatic than the drop in wind speeds that occur between the BULK and SLUCM1. At the rural stations, the SLUCM2 has little impact on the strength of the wind speed (Table 4).

In general, all simulations capture the winds and temperature with reasonable accuracy within the city (Fig. 4). For temperatures, the correlation coefficient falls between 0.99 and 1.0 for all urban land categories, and for the winds, the correlation coefficient varies between 0.90 and 0.95. For temperatures in the rural, COI–HIR, and LIR land categories, the simulations fall very close to the reference circle for the normalized standard deviations (Figs. 4b–d). This indicates that the variability in the simulated temperatures within these land categories is very close to that of the observations. Simulated wind speeds are also highly correlated with the observations (Figs. 4a–d). Overall, the SLUCM1 does the best job in simulating the near-surface winds and temperatures; the BULK configuration overestimates these parameters, and the SLUCM2 underestimates them. It is possible that the SLUCM1 overcorrects (reduces) the 2-m temperature relative to the BULK. Therefore, when the hydrological processes are added in SLUCM2, it further reduces the 2-m temperature, leading to a larger error in this simulation. To further explore such behavior, next we present an analysis of the different components of surface flux that determines the near-surface conditions.

b. *Latent and sensible heat fluxes*

To gain further insight into the variability of the temperature in the simulations, some understanding of the surface evaporation processes and their relationship to the surface energy balance in the city is needed. The surface energy balance in this SLUCM is given by

$$Q_{GH} = Q_{rad} - Q_{LH} - Q_{SH} + Q_{res}, \qquad (1)$$

where Q_{GH} is the ground heat flux, Q_{rad} is the net radiative heat flux, Q_{LH}, Q_{SH}, and Q_{res} are the latent, sensible, and residual heat fluxes, respectively. The combined Q_{LH} and Q_{SH} is denoted as Q_{tur} (turbulent

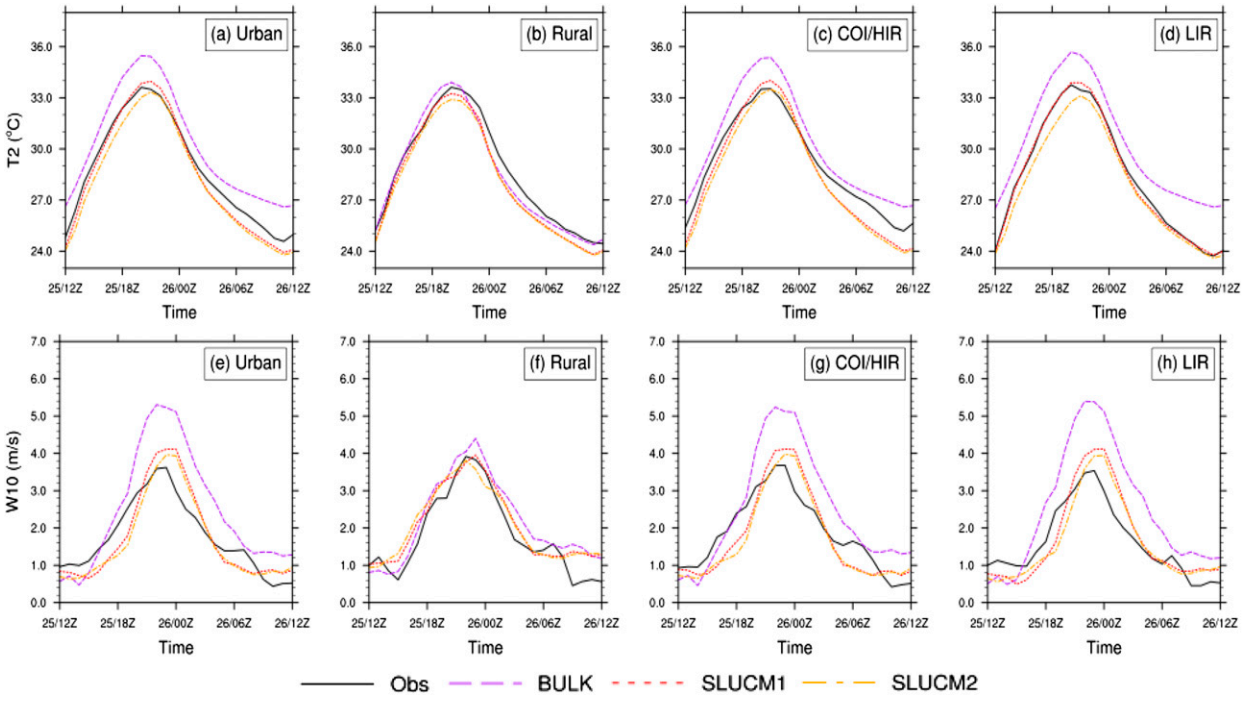

FIG. 3. Observed (black) and simulated (color) 2-m temperature (°C) averaged across all stations for (a) urban land category, (b) rural land category, (c) COI–HIR land category, and (d) LIR land category. (e)–(h) As in (a)–(d), but for 10-m winds ($m\,s^{-1}$).

heat flux). Since the focus of this study is to quantify the relative role of radiative and turbulent flux, we confine our discussions for these two components only. The other terms could be important for a variety of meteorological processes (e.g., Benson-Lira et al. 2016).

We first describe the role of Q_{LH} and Q_{SH} in this section, followed by the role of radiation in section 3c. Figure 5 shows that the BULK Q_{LH} within the urban area is near zero over the three urban categories (Figs. 5a,c,d). In the SLUCM1, the Q_{LH} increases to about 100 $W\,m^{-2}$ around 1900 UTC and then decreases for the urban category (Fig. 5a). In the COI–HIR (Fig. 5c), the maximum Q_{LH} in the SLUCM1 is about 50 $W\,m^{-2}$, whereas in the LIR (Fig. 5d), the Q_{LH} is about 200 $W\,m^{-2}$. In the SLUCM2, the Q_{LH} increases even more within the urban land categories (Figs. 5a,c,d). Overall, the change in Q_{LH} is most dramatic for the stations within the LIR (Fig. 5d). This is because of the relatively low density of artificial surfaces in LIR (50%) in SLUCM in comparison with 100% artificial surfaces in BULK. As expected, at the urban stations, the change in the Q_{SH} is exactly the opposite of the Q_{LH} (Figs. 5e,g,h); that is, as the Q_{SH} decreases, the Q_{LH} increases.

It is interesting to note that there were small changes in the rural areas (Figs. 5b,f) even though there were no changes in the representation of rural pixels in different simulations. This is due to the fact that latent heat flux is a function of wind speed and the humidity difference between the surface and the ambient air above it. Wind speed and the near-surface humidity over the rural areas change because of the presence of urban areas in the model domain. These changes then modify the latent heat flux. Similarly, sensible heat flux is a function of wind speed and temperature difference between the surface and the air above it. As a result, it is expected that there will always be small changes over rural pixels if we have urban pixels in the model domain. To

TABLE 3. RMSE and mean bias of 2-m temperature. The time period for the calculations is from 1200 UTC 25 to 1200 UTC 26 Aug 2000.

	RMSE (°C)				Mean bias (°C)			
	Urban	Rural	COI–HIR	LIR	Urban	Rural	COI–HIR	LIR
Bulk	1.48	0.56	1.21	1.94	1.43	−0.17	1.12	1.87
SLUCM1	0.54	0.68	0.86	0.20	−0.34	−0.57	−0.55	−0.04
SLUCM2	0.79	0.77	1.01	0.66	−0.72	−0.72	−0.83	−0.55

TABLE 4. As in Table 3, but for 10-m wind speeds.

	RMSE ($m\,s^{-1}$)				Mean bias ($m\,s^{-1}$)			
	Urban	Rural	COI–HIR	LIR	Urban	Rural	COI–HIR	LIR
Bulk	1.05	0.49	0.97	1.19	0.73	0.37	0.63	0.87
SLUCM1	0.49	0.41	0.51	0.51	−0.01	0.25	−0.08	0.09
SLUCM2	0.48	0.46	0.53	0.49	−0.10	0.24	−0.18	0.00

illustrate the spatial variability of the Q_{LH} and Q_{SH} in these experiments, next we show their geographical distribution.

In Fig. 6, the Q_{LH} (Figs. 6a,c,e) and Q_{SH} (Figs. 6b,d,f) across Houston are shown at 1900 UTC (1300 CDT). The BULK (Figs. 6a,b) results in a decrease in Q_{LH} and an increase in Q_{SH} across most of the city. The opposite happens in the SLUCM2 (Figs. 6e,f). The decrease in Q_{SH} is most dramatic between the BULK and SLUCM1. These results are consistent with other recent studies (e.g., Miao and Chen 2014).

c. *Relative role of turbulent and radiative fluxes*

To further understand how the surface fluxes are causing the changes in the 2-m and skin temperatures, the surface radiative fluxes are described. The net

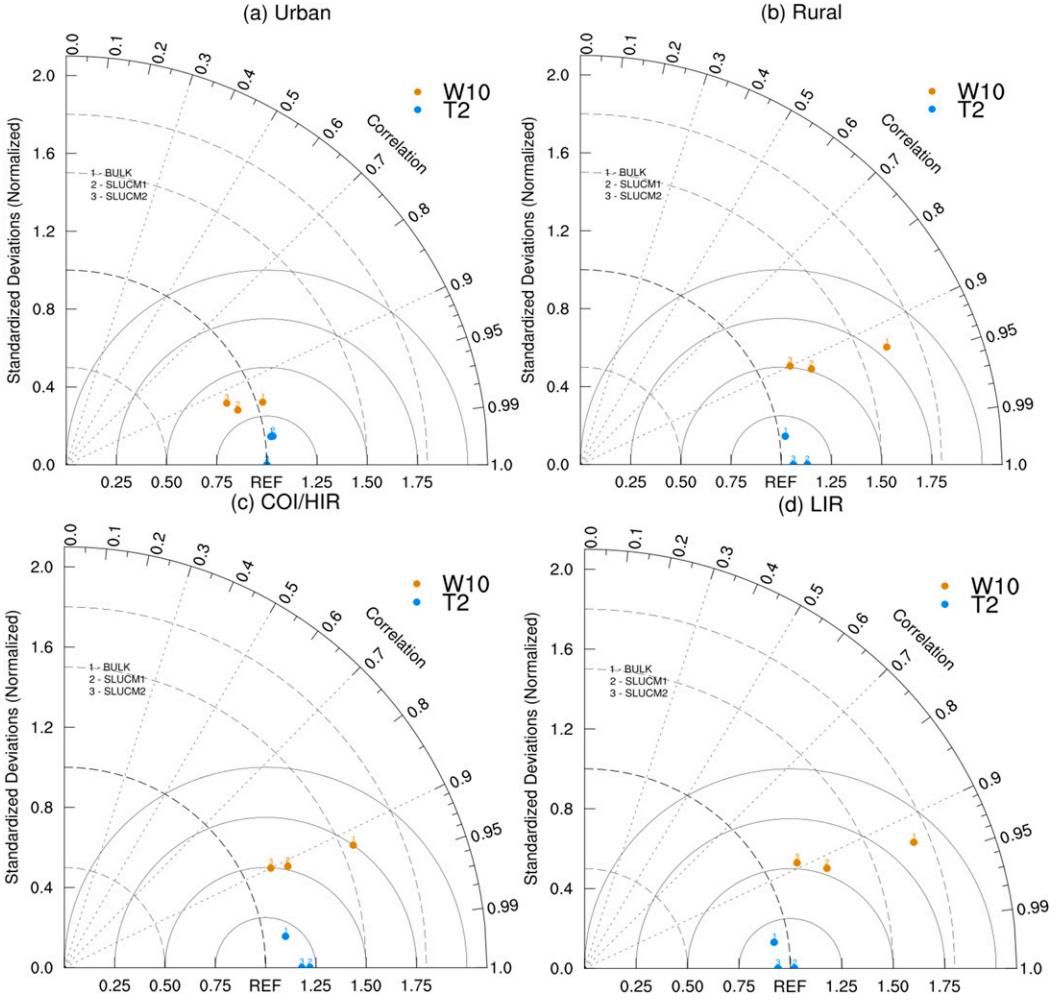

FIG. 4. Taylor diagrams showing the correlation coefficient, normalized standard deviation, and normalized RMS difference for the model's 2-m temperature (T2; blue dots) and 10-m wind speeds (W10; brown dots) for the following land categories: (a) urban, (b) rural, (c) COI–HIR, and (d) LIR.

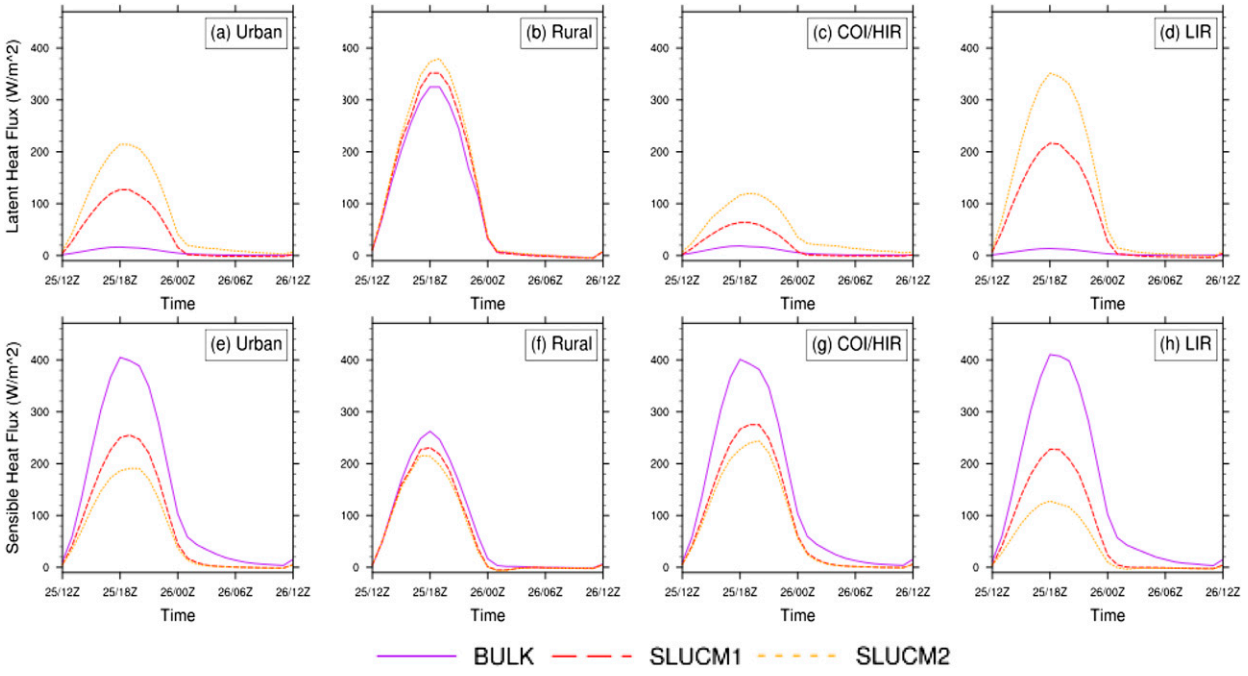

FIG. 5. Averaged surface Q_{LH} (W m^{-2}) from the BULK, SLUCM1, and the SLUCM2 for all (a) urban, (b) rural, (c) COI–HIR, and (d) LIR stations. (e)–(h) As in (a)–(d), but for Q_{SH}.

radiation at the surface, which is a combination of net shortwave and net longwave, can be expressed as

$$Q_{rad} = (Q_{SW}\downarrow - Q_{SW}\uparrow) + (Q_{LW}\downarrow - Q_{LW}\uparrow), \quad (2)$$

$$Q_{SW}\uparrow = \alpha Q_{SW}\downarrow, \quad \text{and} \quad (3)$$

$$Q_{LW}\uparrow = \varepsilon\sigma T_{skin}^4, \quad (4)$$

where $Q_{SW}\downarrow$ represents the incoming shortwave radiation, and $Q_{SW}\uparrow$ represents the outgoing shortwave radiation. Similarly, $Q_{LW}\downarrow$ represents the incoming longwave radiation, and $Q_{LW}\uparrow$ is the outgoing longwave radiation. Equations (2) and (3) were used to calculate the outgoing shortwave and longwave radiation. In these equations, α is the surface albedo, ε is the emissivity, σ is the Stefan–Boltzmann constant, and T_{skin} is the surface skin temperature.

Figure 7 shows the net shortwave (Figs. 7a–d) and the net longwave radiation (Figs. 7e–h) at the surface. The net shortwave is similar in all the simulations because of lack of moist convection and clouds during the simulation period. The BULK has the largest incoming longwave radiation because the BULK has the highest atmospheric temperatures. The BULK skin temperature peaks at 45°C in the urban land category; this is nearly 5°C greater than the peak SLUCM1 skin temperature. In contrast, over the urban land category, the BULK has the lowest absolute values of net longwave radiation (Figs. 7e–h). This is primarily because of the surface emissivity of the BULK rather than that of the SLUCM.

The BULK has less reflected shortwave radiation than the SLUCM experiments. The reflected shortwave radiation is controlled by the surface albedo. During the daytime, the surface albedo in the BULK (0.15) is lower than the SLUCM (0.18) over the urban areas, indicating that the BULK surface is absorbing more incoming shortwave radiation than the SLUCM, causing the net shortwave radiation to be higher than the SLUCM (Figs. 7a–d). Since both the reflected shortwave and upwelling longwave radiation are lowest for the BULK, the overall BULK net surface radiation is larger than the SLUCM for the urban surface (Figs. 8e–h). In comparison, the net turbulent flux in BULK is higher than the SLUCM (Figs. 8a–c) except within the LIR, where the BULK turbulent flux is slightly lower than the SLUCM (Fig. 8d). Despite the very low Q_{LH} in the urban categories, the BULK turbulent flux is higher than the SLUCM turbulent flux because the BULK Q_{SH} is much higher than the SLUCM (Figs. 5e–h). When the radiative and turbulent components of the surface heat budget are taken into account, the BULK heat flux is higher than the SLUCM in the urban land category (Fig. 8i). However, in the COI–HIR land category, the BULK heat flux (i.e., $Q_{rad} - Q_{tur}$) is slightly lower than the SLUCM (Fig. 8l).

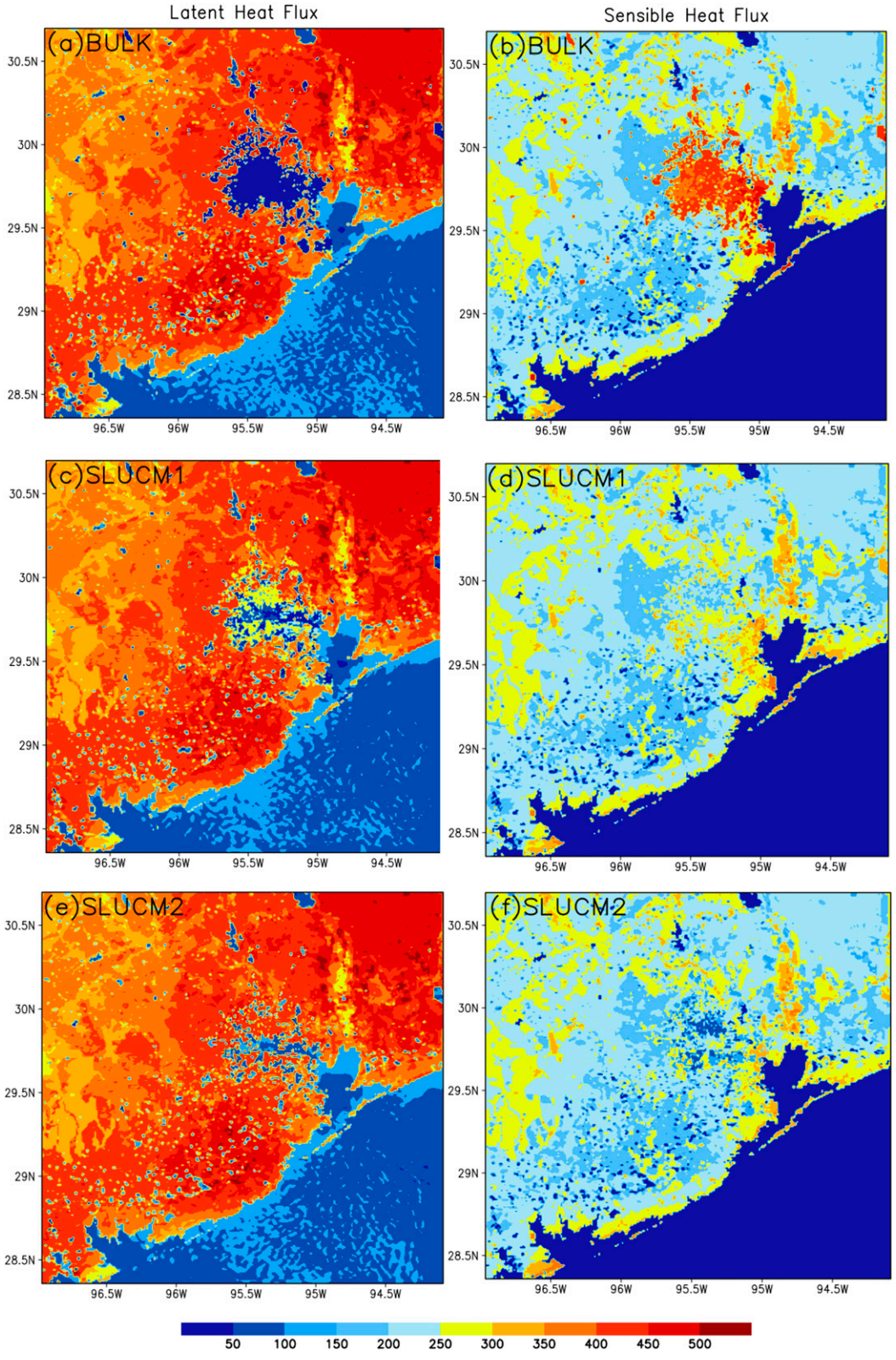

FIG. 6. Surface latent heat flux Q_{LH} (W m^{-2}) from the (a) BULK, (c) SLUCM1, and (e) SLUCM2 in Houston at 1900 UTC (1300 CDT) 25 Aug. (b),(d),(f) As in (a), (c), and (e), but for surface sensible heat flux Q_{SH}.

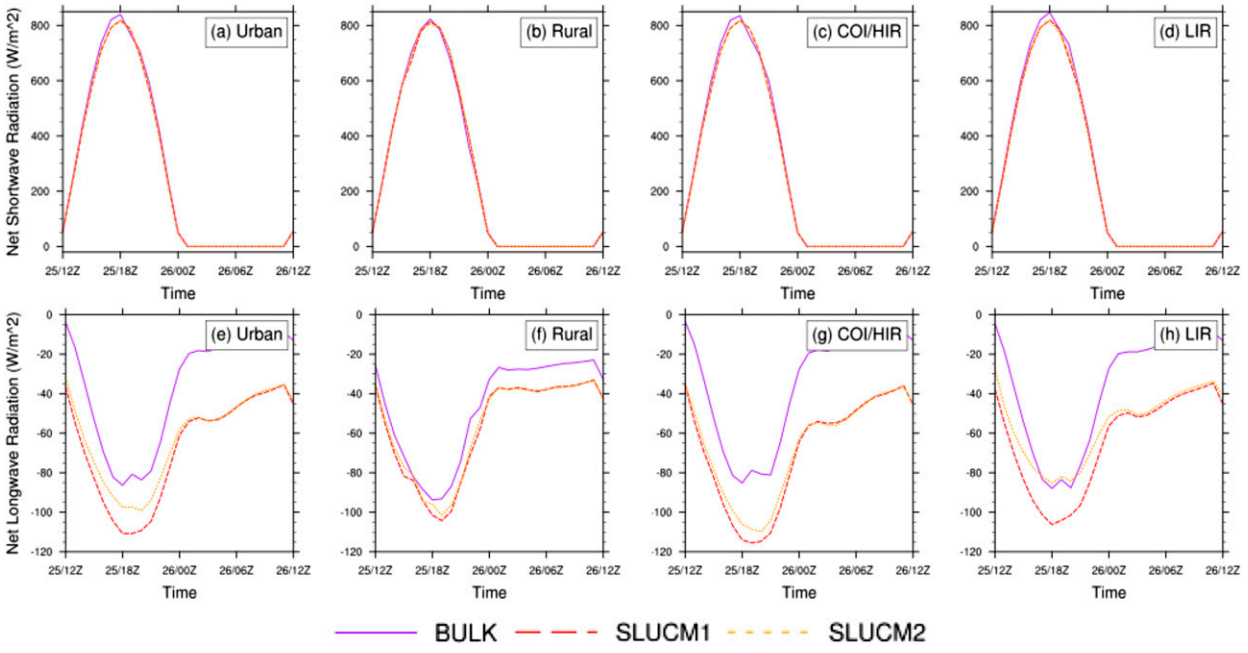

FIG. 7. As in Fig. 5, but for (a)–(d) net shortwave and (e)–(h) net longwave radiation at the surface.

In Fig. 9 and Table 5, the differences (SLUCM1 − BULK; SLUCM2 − SLUCM1) between the radiative and turbulent fluxes are shown to determine whether the radiative or turbulent flux component is contributing more to the near surface temperature changes. The difference between SLUCM1 and BULK (SLUCM2 and SLUCM1) will demonstrate the relative role of turbulent and radiative flux in the absence (presence) of hydrological processes. Within the urban category (Fig. 9a), the net radiation difference between the SLUCM1 and BULK is larger than the net turbulent flux. The average net radiation difference is 36.8 W m^{-2}, and the average net turbulent flux difference is 23.0 W m^{-2} (Table 5). In the LIR land category, this difference is even more extreme as the average net radiation difference is 35.6 W m^{-2}, and the average net turbulent flux difference is 6.9 W m^{-2} (Table 5). These results indicate that changes in the net radiation have a larger impact on the 2-m temperature changes than the net turbulent flux. Hence, much of the temperature change from the BULK to the SLUCM1 is primarily driven by changes in the surface radiative flux; the turbulent flux plays a smaller role.

On the other hand, the average net radiation difference between the SLUCM2 and SLUCM1 is 5.3 W m^{-2}, while the net turbulent flux difference is 15.4 W m^{-2} (Table 5). This trend also occurs within the COI–HIR and LIR land categories. These results suggest that in the presence of urban hydrological processes, the net turbulent flux contributes more to the 2-m temperature change than the net radiative flux. However, changes in the radiative flux cannot be ignored since the change in radiative flux is about one-third of the change in turbulent flux.

The above result is significant because most previous studies about urban parameterization performance and development focus primarily on how the surface turbulent flux changes the near-surface temperature. However, our results indicate that in order to gain a better understanding of the role of surface fluxes, both turbulent and radiative fluxes should be considered. This is especially evident in the absence of the surface urban hydrological processes.

4. Discussion and conclusions

In this study, near-surface temperature and wind speed were evaluated using an improved SLUCM in WRF 3.7. Of the four urban configurations, the BULK overestimated the near-surface temperatures and wind speeds within the urban environment (Fig. 3) and had the largest error (Tables 3 and 4). This is consistent with earlier studies (e.g., Lee et al. 2011; Yang et al. 2014). Even after increasing the amount of surface vegetation and subsequently the Q_{LH} in the city, the BULK still overestimated the UHI effect (Lee et al. 2011).

Between the BULK and SLUCM, there was a noticeable decrease in the 10-m wind speeds in the urban environment. The BULK overestimates the wind speed, whereas SLUCM is much closer to the

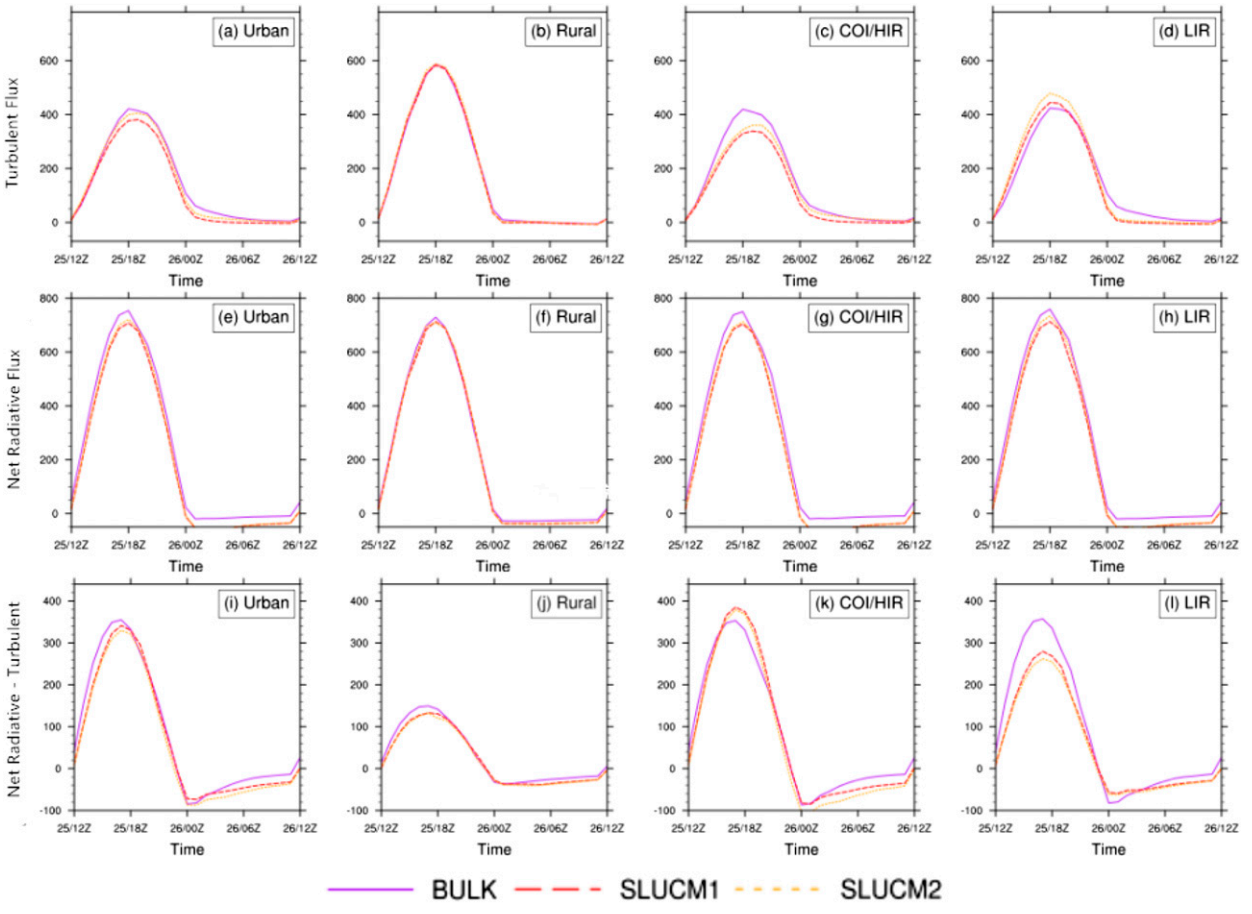

FIG. 8. As in Fig. 5, but for (a)–(d) turbulent flux ($Q_{LH} + Q_{SH}$), (e)–(h) net radiation, and (i)–(l) net heat flux.

observations. This is in contrast to Lee et al. (2011), where the simulated wind speed did not change much between the BULK and SLUCM. The WRF often overestimates the near-surface wind speeds within an urban environment (e.g., Salamanca et al. 2011), which is attributed to a systematic error in WRF (Shimada et al. 2011).

The reason for the changes in the near-surface temperature and wind speeds in the urban environment is directly correlated with the surface heat fluxes since they directly respond to the changes in the urban hydrological processes. As stated before, the original SLUCM in WRF (SLUCM1 in our study) had no urban hydrological processes. As a result, the SLUCM1 underestimates

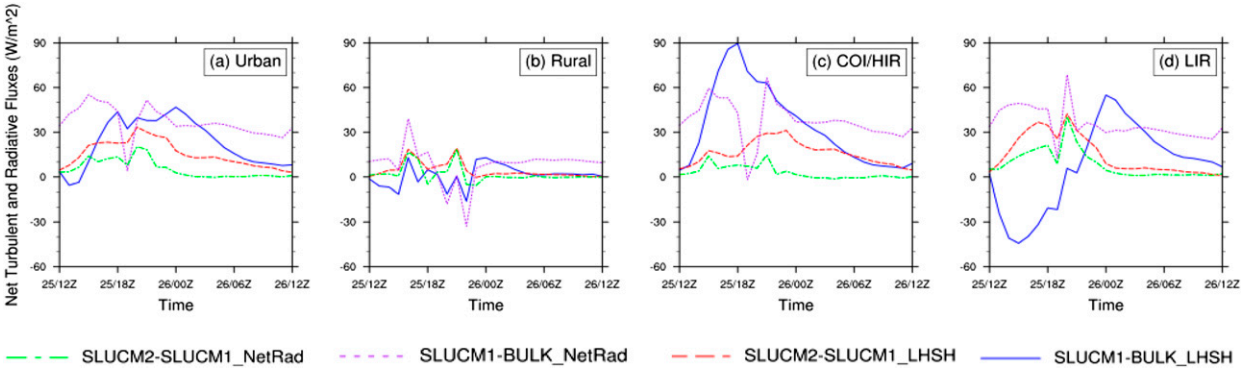

FIG. 9. Net turbulent flux and radiative flux (W m^{-2}) for SLUCM1 minus BULK and SLUCM2 minus SLUCM1 for all land categories.

TABLE 5. SLUCM1 minus BULK and SLUCM2 minus SLUCM1 for turbulent and radiative fluxes ($W\,m^{-2}$). The time period for the calculations is from 1200 UTC 25 to 1200 UTC 26 Aug 2000.

	Urban	Rural	COI–HIR	LIR
SLUCM1 − BULK_LHSH	23.0	1.1	34.4	6.9
SLUCM2 − SLUCM1_LHSH	15.4	4.3	16.1	14.5
SLUCM1 − BULK_NetRad	36.8	8.1	37.7	35.6
SLUCM2 − SLUCM1_NetRad	5.30	1.7	3.0	8.4

the Q_{LH} and overestimates the Q_{SH} (Yang et al. 2015; Miao and Chen 2014). In the presence of urban hydrological processes, there is more surface water and moisture at the city surface. This increase in surface moisture increases the amount of evaporation that occurs at the city surface, and this increases the surface Q_{LH} (Figs. 5a–d). This is consistent with a recent study by Yang et al. (2016) over Houston and Phoenix, Arizona, where the increase in surface moisture was evidenced by the increase in the 2-m dewpoint, although the dewpoint still fell below the observations.

In contrast, there is a low amount of vegetation and no urban hydrological processes in the BULK scheme. This leads to little surface moisture in the city and results in very low Q_{LH} and very high Q_{SH} (Fig. 6). With little to no Q_{LH}, the surface and near-surface temperatures in the urban area increase above the observations (Figs. 3a,c,d). This combination of higher temperatures and a very dry urban surface cause elevated surface Q_{SH}. This is known to occur because surfaces like dry soil have a very low thermal conductivity, so the thermal energy released by the high temperatures is not absorbed into the ground but rather up into the atmosphere as enhanced sensible heat fluxes (Chen et al. 2011b). The increase in surface temperature enhances thermals over the urban areas, which in turn increases the vertical motion over the city (e.g., Chen et al. 2011b; Grimmond et al. 2010, 2011; Miao and Chen 2014).

In the presence of urban hydrological processes, the rate of surface evaporation increases, and this causes the temperature to decrease in the model. As the Q_{LH} increases (Fig. 5) in the city, the amount of cooling at the city surface increases (Fig. 3). Although the best correlation between temperature changes and surface fluxes should be inferred from surface skin temperatures, it is interesting that as the Q_{LH} increases with each urban configuration, the 2-m temperatures do decrease within the city. This decrease in temperature is also clearly demonstrated with the skin temperature (not shown). As with the 10-m wind speeds and 2-m temperatures, the most dramatic decrease occurs between the BULK and SLUCM1 (not shown).

Our original hypothesis, that the updated SLUCM with urban hydrological processes would decrease the near-surface temperature simulations, proved to be correct. However, the error in the near-surface temperature simulations higher because of too much cooling in the presence of urban hydrological processes. In other words, the simulated temperature in the city decreases below the observations in the presence of hydrological processes, which causes the RMSE and mean bias to increase more than the SLUCM without hydrological processes. This is in contrast to Chen et al. (2011b), who found temperatures that were nearly 1°C higher than the observations. Although it is impossible to find the exact cause for such discrepancy, there are some possibilities:

(i) To what extent our results are dependent on the chosen set of schemes in the WRF is not known and needs to be verified in the future. During our initial tests over Houston, we tried many different combinations that did not produce any significantly different results. This is possibly due to our choice of the simulation time that was free from weather disturbances. It would be interesting to find whether these results will hold in the presence of moist convection.

(ii) We have used the default options for urban hydrological processes in the simulations. Whether these options are applicable to Houston at the chosen simulation period or needs modification is not known at this time. For example, Lee et al. (2011) modified different parameters to use the SLUCM over Houston and found only slight improvements in their results. To what extent our simulations will be modified by the use of Lee et al.'s (2011) recommended parameters needs to be studied in the future. As a result, validation studies using the improved SLUCM should be carried out at different cities around the United States and the world under different meteorological conditions. Such analyses are beyond the scope of this paper.

Our results show that apart from latent and sensible heat fluxes, radiative fluxes can also play a significant role on changes in temperature and winds. In the BULK, upwelling shortwave and longwave radiation are smaller than the SLUCM. For the shortwave radiation, this is because the BULK surface albedo is lower during the day than the SLUCM albedo. As a result, the surface albedo seems to play a significant role in determining the surface heat fluxes and, hence, the near-surface temperature at the urban areas (Takebayashi and Moriyama 2012). The upwelling longwave radiation in the BULK is also less because the surface emissivity is lower in the BULK than the SLUCM simulations. These two factors

cause the BULK to have higher urban temperatures than the SLUCM experiments.

Our results also indicate that in the presence of urban hydrological processes, the turbulent flux contributes more to the 2-m temperature changes than the radiative flux. However, in the absence of hydrological processes, radiative flux contributes more to the 2-m temperature changes than the turbulent flux. This is a significant result as it shows that the changes in the net radiation cannot be ignored. Most studies relevant to the use of urban parameterizations previously focused on the turbulent flux only. Our results show that to get a better understanding of the relationship between surface heat fluxes and near-surface temperature changes, contributions from both turbulent and radiative fluxes need to be considered.

Acknowledgments. The simulations were conducted at the Florida Institute of Technology using the high-performance computing cluster Blueshark, which was funded by the NSF. The first author JB greatly acknowledges AMS for supporting his travel to present this research in the 2016 AMS Annual Meeting. This work was partially supported by grants from the NSF (1323400) and the ONR (N00014-16-1-3091) to PR. We thank comments from Steven Lazarus on an earlier version of this paper. We also thank four anonymous reviewers and the editor (Dr. Bart Geerts) for their constructive comments that improved this paper significantly.

REFERENCES

Benson-Lira, V., M. Georgescu, S. Kaplan, and E. R. Vivoni, 2016: Loss of a lake system in a megacity: The impact of urban expansion on seasonal meteorology in Mexico City. *J. Geophys. Res. Atmos.*, **121**, 3079–3099, doi:10.1002/2015JD024102.

Bornstein, R. D., and Q. L. Lin, 2000: Urban heat islands and summertime convective thunderstorms in Atlanta: Three case studies. *Atmos. Environ.*, **34**, 507–516, doi:10.1016/S1352-2310(99)00374-X.

Bueno, B., G. Pigeon, L. K. Norford, K. Zibouche, and C. Marchadier, 2012: Development and evaluation of a building energy model integrated in the TEB scheme. *Geosci. Model Dev.*, **5**, 433–448, doi:10.5194/gmd-5-433-2012.

Chen, F., and J. Dudhia, 2001: Coupling an advanced land surface–hydrology model with the Penn State–NCAR MM5 modeling system. Part I: Model implementation and sensitivity. *Mon. Wea. Rev.*, **129**, 569–585, doi:10.1175/1520-0493(2001)129<0569:CAALSH>2.0.CO;2.

——, H. Kusaka, M. Tewari, J. W. Bao, and H. Hirakuchi, 2004: Utilizing the coupled WRF/LSM/urban modeling system with detailed urban classification to simulate the urban heat island phenomena over the greater Houston area. *Fifth Symp. on the Urban Environment*, Vancouver, BC, Canada, Amer. Meteor. Soc., 9.11. [Available online at https://ams.confex.com/ams/AFAPURBBIO/techprogram/paper_79765.htm.]

——, and Coauthors, 2011a: The integrated WRF/urban modelling system: Development, evaluation, and applications to urban environmental problems. *Int. J. Climatol.*, **31**, 273–288, doi:10.1002/joc.2158.

——, S. Miao, M. Tewari, J. W. Bao, and H. Kusaka, 2011b: A numerical study of interactions between surface forcing and sea breeze circulations and their effects on stagnation in the greater Houston area. *J. Geophys. Res.*, **116**, D12105, doi:10.1029/2010JD015533.

Cheng, F. Y., and D. W. Byun, 2008: Application of high resolution land use and land cover data for atmospheric modeling in the Houston–Galveston metropolitan area, part I: Meteorological simulation results. *Atmos. Environ.*, **42**, 7795–7811, doi:10.1016/j.atmosenv.2008.04.055.

Craig, K. J., and R. D. Bornstein, 2002: MM5 simulation of urban induced convective precipitation over Atlanta. Preprints, *Fourth Symp. on the Urban Environment*, Norfolk, VA, Amer. Meteor. Soc., 1.3. [Available online at https://ams.confex.com/ams/AFMAPUE/webprogram/Paper38803.html.]

Deardorff, J. W., 1978: Efficient prediction of ground surface temperature and moisture, with inclusion of a layer of vegetation. *J. Geophys. Res.*, **83**, 1889–1903, doi:10.1029/JC083iC04p01889.

Dudhia, J., 1989: Numerical study of convection observed during the Winter Monsoon Experiment using a mesoscale two–dimensional model. *J. Atmos. Sci.*, **46**, 3077–3107, doi:10.1175/1520-0469(1989)046<3077:NSOCOD>2.0.CO;2.

Georgescu, M., M. Moustaoui, A. Mahalov, and J. Dudhia, 2011: An alternative explanation of the semiarid urban area ''oasis effect.'' *J. Geophys. Res.*, **116**, D24113, doi:10.1029/2011JD016720.

Grimmond, C. S. B., and Coauthors, 2010: The international urban energy balance models comparison project: First results from phase 1. *J. Appl. Meteor. Climatol.*, **49**, 1268–1292, doi:10.1175/2010JAMC2354.1.

——, and Coauthors, 2011: Initial results from phase 2 of the international urban energy balance model comparison. *Int. J. Climatol.*, **31**, 244–272, doi:10.1002/joc.2227.

Hjelmfelt, M. R., 1982: Numerical simulation of the effects of St. Louis on mesoscale boundary-layer airflow and vertical air motion: Simulations of urban vs non-urban effects. *J. Appl. Meteor.*, **21**, 1239–1257, doi:10.1175/1520-0450(1982)021<1239:NSOTEO>2.0.CO;2.

Hong, S.-Y., J. Dudhia, and S.-H. Chen, 2004: A revised approach to ice microphysical processes for the bulk parameterization of clouds and precipitation. *Mon. Wea. Rev.*, **132**, 103–120, doi:10.1175/1520-0493(2004)132<0103:ARATIM>2.0.CO;2.

Janjić, Z. I., 1994: A step-mountain eta coordinate model: Further developments of the convection, viscous sub layer, and turbulence closure schemes. *Mon. Wea. Rev.*, **122**, 927–945, doi:10.1175/1520-0493(1994)122<0927:TSMECM>2.0.CO;2.

Kain, J. S., 2004: The Kain–Fritsch convective parameterization: An update. *J. Appl. Meteor.*, **43**, 170–181, doi:10.1175/1520-0450(2004)043<0170:TKCPAU>2.0.CO;2.

Kalnay, E., and M. Cai, 2003: Impact of urbanization and land-use change on climate. *Nature*, **423**, 528–531, doi:10.1038/nature01675.

Kusaka, H., H. Kondo, Y. Kikegawa, and F. Kimura, 2001: A simple single-layer urban canopy model for atmospheric models: Comparison with multilayer and slab models. *Bound.-Layer Meteor.*, **101**, 329–358, doi:10.1023/A:1019207923078.

Lee, S. H., and S. U. Park, 2008: A vegetated urban canopy model for meteorological and environmental modelling. *Bound.-Layer Meteor.*, **126**, 73–102, doi:10.1007/s10546-007-9221-6.

——, and Coauthors, 2011: Evaluation of urban surface parameterizations in the WRF Model using measurements during the Texas Air Quality Study 2006 field campaign. *Atmos. Chem. Phys.*, **11**, 2127–2143, doi:10.5194/acp-11-2127-2011.

Liu, Y., F. Chen, T. Warner, and J. Basara, 2006: Verification of a mesoscale data-assimilation and forecasting system for the Oklahoma City area during the Joint Urban 2003 field project. *J. Appl. Meteor. Climatol.*, **45**, 912–929, doi:10.1175/JAM2383.1.

Martilli, A., A. Clappier, and M. W. Rotach, 2002: An urban surface exchange parameterization for mesoscale models. *Bound.-Layer Meteor.*, **104**, 261–304, doi:10.1023/A:1016099921195.

Mestayer, P. G., and Coauthors, 2005: The urban boundary-layer field campaign in Marseille (UBL/CLU-ESCOMPTE): Set-up and first results. *Bound.-Layer Meteor.*, **114**, 315–365, doi:10.1007/s10546-004-9241-4.

Miao, S., and F. Chen, 2014: Enhanced modeling of latent heat flux from urban surfaces in the Noah/single-layer urban canopy coupled model. *Sci. China Earth Sci.*, **57**, 2408–2416, doi:10.1007/s11430-014-4829-0.

Mlawer, E. J., S. J. Taubman, P. D. Brown, M. J. Iacono, and S. A. Clough, 1997: Radiative transfer for inhomogeneous atmospheres: RRTM, a validated correlated-*k* model for the longwave. *J. Geophy. Res.*, **102**, 16 663–16 682, doi:10.1029/97JD00237.

Moriwaki, R., M. Kanda, H. Senoo, A. Hagishima, and T. Kinouchi, 2008: Anthropogenic water vapor emissions in Tokyo. *Water Resour. Res.*, **44**, W11424, doi:10.1029/2007WR006624.

Nielsen-Gammon, J. W., 2002: Evaluation and comparison of preliminary meteorological modeling for the August 2000 Houston–Galveston ozone episode. Texas Natural Resource Conservation Commission Rep., 83 pp.

Oke, T. R., 1979: Advectively-assisted evapotranspiration from irrigated urban vegetation. *Bound.-Layer Meteor.*, **17**, 167–173, doi:10.1007/BF00117976.

Oleson, K. W., G. B. Bonan, J. Feddema, M. Vertenstein, and C. S. B. Grimmond, 2008: An urban parameterization for a global climate model. Part 1: Formulation and evaluation for two cities. *J. Appl. Meteor. Climatol.,*, **47**, 1038–1060, doi:10.1175/2007JAMC1597.1.

Ramamurthy, P., and E. Bou-Zeid, 2014: Contribution of impervious surfaces to urban evaporation. *Water Resour. Res.*, **50**, 2889–2902, doi:10.1002/2013WR013909.

Rotach, M. W., and Coauthors, 2005: BUBBLE—An urban boundary layer meteorology project. *Theor. Appl. Climatol.*, **81**, 231–261, doi:10.1007/s00704-004-0117-9.

Rozoff, C. M., W. R. Cotton, and J. O. Adegoke, 2003: Simulation of St. Louis, Missouri, land use impacts on thunderstorms. *J. Appl. Meteor.*, **42**, 716–738, doi:10.1175/1520-0450(2003)042<0716:SOSLML>2.0.CO;2.

Salamanca, F., A. Martilli, M. Tewari, and F. Chen, 2011: A study of the urban boundary layer using different urban parameterizations and high-resolution urban canopy parameters with WRF. *J. Appl. Meteor. Climatol.*, **50**, 1107–1128, doi:10.1175/2010JAMC2538.1.

Sharma, A., P. Conry, H. J. S. Fernando, A. F. Hamlet, J. J. Hellmann, and F. Chen, 2016: Green and cool roofs to mitigate urban heat island effects in the Chicago metropolitan area: Evaluation with a regional climate model. *Environ. Res. Lett.*, **11**, 064004, doi:10.1088/1748-9326/11/6/064004.

Shimada, S., T. Ohsawa, S. Chikaoka, and K. Kozai, 2011: Accuracy of the wind speed profile in the lower PBL as simulated by the WRF Model. *SOLA*, **7**, 109–112, doi:10.2151/sola.2011-028.

Skamarock, W. C., and Coauthors, 2008: A description of the Advanced Research WRF version 3. NCAR Tech. Note NCAR/TN-4751+STR, 113 pp., doi:10.5065/D68S4MVH.

Takebayashi, H., and M. Moriyama, 2012: Study on surface heat budget of various pavements for urban heat island mitigation, *Adv. Mater. Sci. Eng.*, **2012**, 523051, doi:10.1155/2012/523051.

Tewari, M., and Coauthors, 2004: Implementation and verification of the unified Noah land surface model in the WRF Model. *20th Conf. on Weather Analysis and Forecasting/16th Conf. on Numerical Weather Prediction*, Seattle, WA, Amer. Meteor. Soc., 14.2a. [Available online at https://ams.confex.com/ams/84Annual/techprogram/paper_69061.htm.]

Walko, R. L., and Coauthors, 2000: Coupled atmosphere–biophysics–hydrology models for environmental modeling. *J. Appl. Meteor.*, **39**, 931–944, doi:10.1175/1520-0450(2000)039<0931:CABHMF>2.0.CO;2.

Wang, Z. H., E. Bou-Zeid, and J. A. Smith, 2011: A spatially-analytical scheme for surface temperatures and conductive heat fluxes in urban canopy models. *Bound.-Layer Meteor.*, **138**, 171–193, doi:10.1007/s10546-010-9552-6.

——, ——, and ——, 2013: A coupled energy transport and hydrological model for urban canopies evaluated using a wireless sensor network. *Quart. J. Roy. Meteor. Soc.*, **139**, 1643–1657, doi:10.1002/qj.2032.

Weaver, C. P., and Coauthors, 2009: A preliminary synthesis of modeled climate change impacts on U.S. regional ozone concentrations. *Bull. Amer. Meteor. Soc.*, **90**, 1843–1863, doi:10.1175/2009BAMS2568.1.

Westcott, N. E., 1995: Summertime cloud-to-ground lightning activity around major midwestern urban areas. *J. Appl. Meteor.*, **34**, 1633–1642, doi:10.1175/1520-0450-34.7.1633.

Yang, J., Z. H. Wang, F. Chen, S. Miao, M. Tewari, J. A. Voogt, and S. Myint, 2015: Enhancing hydrologic modelling in the coupled Weather Research and Forecasting–Urban Modelling System. *Bound.-Layer Meteor.*, **155**, 87–109, doi:10.1007/s10546-014-9991-6.

——, ——, M. Georgescu, F. Chen, and M. Tewari, 2016: Assessing the impact of enhanced hydrological processes on urban hydrometeorology with application to two cities in contrasting climates. *J. Hydrometeor.*, **17**, 1031–1047, doi:10.1175/JHM-D-15-0112.1.

Yang, L., J. A. Smith, M. L. Baeck, E. Bou-Zeid, S. M. Jessup, F. Tian, and H. Hu, 2014: Impact of urbanization on heavy convective precipitation under strong large-scale forcing: A case study over the Milwaukee–Lake Michigan region. *J. Hydrometeor.*, **15**, 261–278, doi:10.1175/JHM-D-13-020.1.

Zhang, D.-L., Y. X. Shou, R. R. Dickerson, and F. Chen, 2011: Impact of upstream urbanization on the urban heat island effects along the Washington–Baltimore corridor. *J. Appl. Meteor. Climatol.*, **50**, 2012–2029, doi:10.1175/JAMC-D-10-05008.1.